A Multi-Source Energy Harvesting System to Power Microcontrollers for Cryptography

Jiayu Li, Ji Hoon Hyun, and Dong Sam Ha
Bradley Department of Electrical and Computer Engineering
Virginia Polytechnic Institute and State University
Balcksburg, USA
{jli4, jhyun, ha}@vt.edu

Abstract— This paper presents a multi-source energy harvesting system for vibration, thermal, and solar energy from automobiles, which aims to power a microcontroller (MCU) for cryptography. Each building block adopts a maximum power extraction scheme to match the unique characteristic of the energy source. Resistive impedance matching with a buck-boost converter is adopted for vibration and thermal energy harvesting, and maximum power point tracking for solar energy harvesting. The proposed system provides two regulated voltages, 3.3 V and 5 V, to power an MCU. An energy level indicator indicates the current energy level stored in the storage device. The MCU processes a cryptography algorithm accordingly based on the current energy level. The system is able to cold start, i.e., even if the storage device is drained completely, it can start.

Keywords—Automobile energy harvesting, vibration energy harvesting, thermal energy harvesting, solar energy harvesting, wake-up circuit, impedance matching, maximum power point tracking

I. INTRODUCTION

The internet of thing (IoT) is the internetworking of physical devices embedded with sensors, actuators, and network connectivity that enable these objects to collect and exchange data. The number of IoT devices will reach 50 billion objects by 2020, among which more than 30 billion devices will be wirelessly connected [1], [2]. A key requirement for massive deployment of wireless IoT devices is autonomous power, in which an IoT device, powered up by energy harvested from ambient sources, can operate perpetually. Replacing batteries for wireless IoT devices is inconvenient, expensive, or impractical for such applications. Energy harvesting from ambient sources offers a promising solution.

Typical ambient energy sources include solar, vibration and oscillation, thermal, and RF. Researchers developed energy harvesting circuits to harvest from multiple energy sources [3], [4], [5], [6]. Bandyopadhyay and Chandrakasan fabricated an integrated circuit to harvest solar, thermal, and vibration energy, in which the inductor is shared [3]. Ding et al. developed multi-source energy harvesting system for in-door light, thermal and vibration, which aims to power non-volatile processors [4]. Alhawari et al. developed a power management unit to harvest vibration and thermal energy for wearable devices [5]. Our team presented an energy harvesting system to harvest vibration and thermal energy from car batteries of

electric vehicles [6]. This paper is extension of our work, which adds solar energy harvesting in addition to vibration and thermal energy.

Ambient energy sources may not be available continuously and typically intermittent. A good example is solar energy which is available during day time. It is reported that privately-owned cars are parked about 95% of the time [7]. Energy from wearable devices such as shoes and backpacks are intermittent [8]. An important design issue for energy harvesting circuit is to minimize the power dissipation when the ambient energy is unavailable. Toward the objective, we adopted a wake-up circuit, which monitors availability of the source energy continuously [6], [9], [10], [11]. Upon detection of the energy, it wakes up and starts to harvest energy. Otherwise, the circuit is in sleep mode to minimize the power dissipation. The proposed circuit also adopts a wake-up circuit.

Suslowicz et al. consider the optimization of cryptographic protocols under energy harvesting conditions [12]. When there is harvested energy available, but there are no useful operations to complete. This can occur in cryptographic protocols, while the protocol waits for the next message. To avoid waste, they partition cryptographic algorithms into an offline portion and an online portion, where only the online portion has a real-time dependency to the availability of data. The offline portion is precomputed with the result stored as a coupon for the remaining online operation. To enable such optimization, the system requires to know the level of energy stored in the storage device, i.e., super capacitor. The proposed circuit adopts an energy level indicator, which indicates the level of available energy based on the voltage of the capacitor.

The paper is organized as follows. Section II describes preliminary materials, specifically transducers for energy harvesting, an active rectifier, and impedance matching. Section III presents the proposed circuit including key building blocks and their operations. Section IV presents the experiment setup and experimental results. Section V draws a conclusion.

II. PRELIMINARIES

A. Transducers for Energy Harvesting

Photovoltaic (PV) cells are used for solar energy harvesting, piezoelectric cantilevers are often for vibration energy harvesting, and thermoelectric generators for thermal energy harvesting. PV cells offer highest energy density among the three transducers. The maximum power point of a PV cell depends on the irradiance level, which requires to keep track of the maximum power point for high efficiency [13]. A piezoelectric cantilever, generally made of a ceramic material such as lead-zirconate-titanate (PZT), is most efficient when operating at the resonant frequency [14]. A PZT cantilever generates relatively high ac voltage, requiring a rectifier. A resistive matching is often adopted for a PZT cantilever operating at the resonant frequency. A thermoelectric generator (TEG) for thermal energy harvesting generates relatively low dc voltage. The internal impedance of a TEG is resistive and hardly affected by the operating condition. So, resistive impedance matching is usually used for TEGs.

B. Negative Voltage Converter

A PZT cantilever generates ac voltage to require a rectifier. A full bridge rectifier composing four passive diodes such as Schottky diodes are commonly used for high power applications. The voltage drop across passive diodes and hence power dissipation of the rectifier is relatively high for a smallscale energy harvesting system. The negative voltage converter (NVC) topology shown in Fig. 1 is composed of an NMOS transistor pair and a PMOS transistor pair with the gates of each pair connected to the opposite input source terminals [15]. The currents flow for both the positive cycle and the negative cycle is indicated in Fig. 1. The current flows into the output terminal in the same direction, and hence the ac voltage is rectified through four transistors.

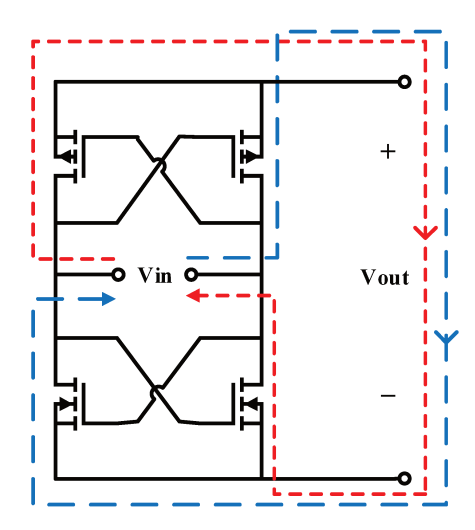


Fig. 1. Negative voltage converter.

C. Buck-boost convert in DCM

An inverting buck-boost converter is shown in the Fig. 2. Since the switching frequency of a buck-boost converter is much higher than the vibration frequency, the input voltage can be treated as dc voltage for each switching cycle. Note that the polarity of the output voltage is opposite to the input voltage. The emulated input resistance R_{in} of a buck-boost converter in discontinuous conduction mode (DCM) can be expressed in (1).

$$R_{in} = \frac{2L}{D^2 T_{\rm s}} \tag{1}$$

where L is the inductance, D the duty cycle, and T_s the switching period of the converter. The emulated input impedance is independent of the load condition, input and output voltages, which is a major advantage of a buck-boost converter in DCM [14], [15]. This topology is adopted for a PZT cantilever and a TEG for our system.

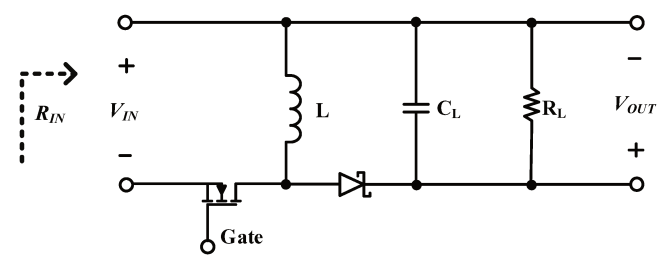


Fig. 2. Buck-boost converter.

The oscillator used to generate the desired duty cycle waveform consists of RC networks and an ultra-low power dissipation comparator [16]. The output frequency and duty cycle could be determined by changing the values of R₁, R₂, and the capacitor. The output V_{OUT} is tied to the gate terminal of the MOSFET.

D. Osicillator

The oscillator shown in Fig. 3 generates a switching frequency with a fixed duty cycle, which switches the converter [17]. The operation of the oscillator is as follows. . Suppose that the output voltage of the comparator is V_{WAKE} initially. As the capacitor C is charged through R_1 and R_2 , and its voltage increases toward (2/3)V_{WAKE}, When the voltage reaches at (2/3)V_{WAKE}, the comparator output becomes low. Now, the capacitor starts to discharge through R₂. When the capacitor voltage reaches (1/3)V_{WAKE}, the comparator output becomes low. Now, the capacitor starts to discharge through R₂. When the capacitor voltage reaches (1/3)V_{BATT}, the comparator output becomes high, and the cycle repeats. The frequency and the duty cycle of the oscillator can be approximated as shown in (2) and (3) if R₂ is much larger than R₁ [17]. The duty cycle and switching frequency can be tuned by the R₁, R₂ and C. In practice, either R₁ and R₂ can be a variable resistor to make the oscillator tunable. The output voltage V_{GATE} drives the gate of the buck-boost converter.

$$D \approx \frac{R_1}{R_2} \tag{2}$$

$$D \approx \frac{R_1}{R_2}$$

$$F_s \approx \frac{1}{(R_1 + R_2)C \ln 2}$$
(2)

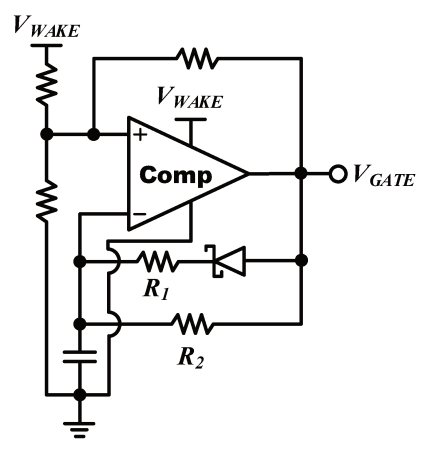


Fig. 3. Oscillator.

III. PROPOSED ENERGY HARVESTING SYSTEM

This section describes the proposed energy harvesting system with the target energy source of automobiles. It presents overall operation and major building blocks.

A. Overview

A PZT cantilever for vibration energy harvesting, a TEG for thermal energy, and PV cell for solar energy are used for the proposed energy harvesting system shown in Fig. 4. The dashed lines in the figure show the flow of the harvested energy. As a vehicle starts to move, the PZT cantilever generates voltage. The wake-up circuit senses the voltage and activates the PZT oscillator. The PZT buck-boost converter starts to harvest vibration energy. When the vehicle is turned off, the wake-up circuit deactivates the oscillator and the converter to save power. As thermal energy is available only when a vehicle is moving, the wake-up circuit is shared with the TEG. In other word, as a vehicle starts to move, the TEG converter is activated and starts to harvest the thermal energy. However, the PV cell has its own dedicated wake-up/sleep mode controller.

A dedicated buck-boost converter with an associated oscillator provides resistive matching for the PZT cantilever, and it is the same for a TEG. A dedicated off-the-shelf IC, Texas Instruments, BQ25504, provides impedance matching for the PV cell. The energy harvested from three different sources charge the same storage device, the super capacitor C_B. The two buck converters in series provide regulated voltages, 3.3 V and 5 V, for an MCU. The "Energy Level Indicator" senses the capacitor voltage and set the two outputs appropriately depending on the sensed voltage. The two outputs indicate the level of the energy stored in the capacitor, which is used for the MCU to select necessary computation for the cryptography algorithm

B. Wake-up Circuit and Cold Start

The wake-up circuit is shown in Fig. 5. The input V_{in} is the rectified PZT voltage, i.e., the output of the NVC in Fig. 1. The Zenor diode D_1 limits the input voltage to 5 V, which aims to protect the comparator. When the PZT cantilever starts to generate energy, i.e., voltage, it starts charging capacitor C_1 . Once the voltage V_{WAKE} PZT of C_1 reaches 0.9 V, the comparator for the PZT oscillator is activated. When the capacitor voltage becomes higher than the built-in offset voltage, the comparator output V_{WAKE} TEG becomes high to activate the TEG oscillator. (Refer to Fig. 3 for the oscillator circuit.) An active oscillator activates the associated buck-boost converter by switching the MOSFET, which in turn starts to harvest energy.

The proposed circuit is able to cold start. Suppose the super capacitor C_B is completely drained, implying the supply voltage V_{DD} is 0 V. When the PZT cantilever generates ac voltage, it starts to charge the capacitor C_1 . When the capacitor voltage reaches 0.9 V, the PZT oscillator is activated, and hence the PZT buck-boost converter. When the voltage of the super capacitor C_B reaches 1.6 V, the comparator of the wake-up circuit is activated, and the output voltage V_{WAKE_TEG} becomes high to activate the TEG oscillator and hence the TEG converter.

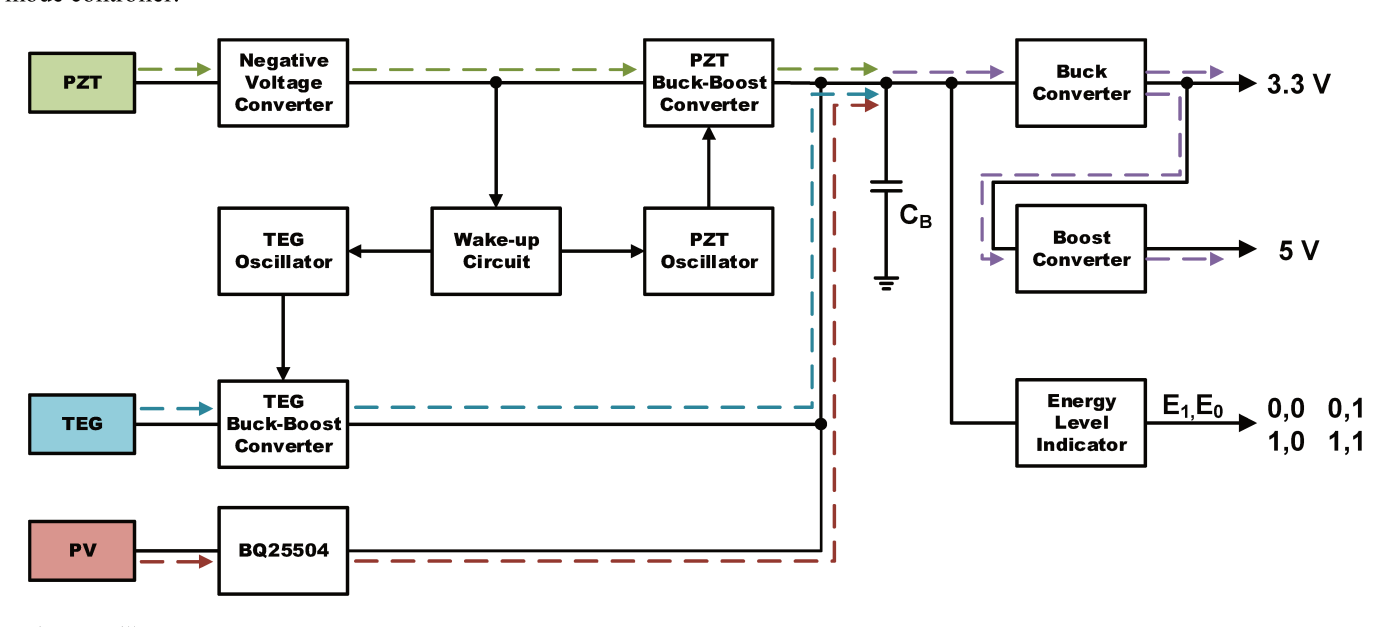


Fig. 4. Oscillator.

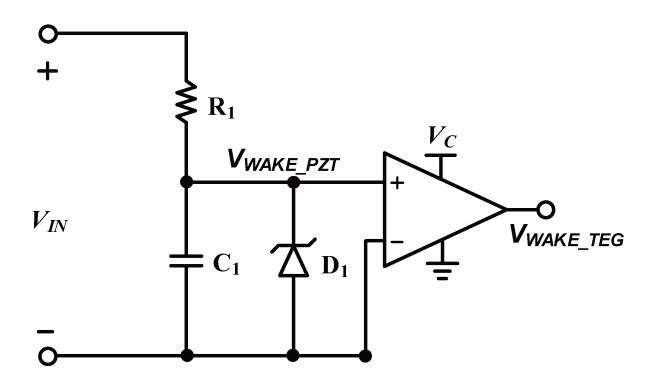


Fig. 5. Wake-up circuit.

C. Impedance Matching and Maximum Power Point Tracking

Assuming the PZT cantilever vibrates at the resistance, the associated buck-boost converter in DCM performs fixed resistive impedance matching, i.e., the converter emulates fixed resistance equal to the source resistance. It is the same for the TEG buck-boost converter; a buck-boost converter provides fixed resistive matching.

Texas Instruments BQ25504 is used for impedance matching for the PV cell [18]. BQ25504 based on a boost converter intends for low power energy harvesting for solar and thermal energy. It performs maximum power point tracking (MPPT) based on fractional open circuit voltage (FOCV). The harvester cuts off the load every 16 seconds for 256 milliseconds to measure the open circuit voltage. Then, it reconnects the load and adjusts the load voltage to 70% to 80% of the open-circuit voltage for PV cell. The fraction can be adjusted with external resistors, and it is set to 75% for the proposed system.

D. Energy Level Indicator

The energy level stored in a capacitor C is expressed in (4).

$$E = \frac{1}{2}CV_C^2 \tag{4}$$

where V_{C} is the capacitor voltage. The Energy Level Indicator senses the capacitor voltage and indicate energy level in four different steps, $E_1E_0 = 00, 01, 10, 11, in which 00 (11)$ indicates the lowest (highest) energy level. The proposed energy level indicator shown in Fig. 6 consists of an inverting amplifier, three voltage detector ICs, and logic gates. The voltage detector TPS3779 compares the applied input voltage with its internal reference voltage or threshold voltage. The input voltage is higher (lower) than the threshold voltage, the output becomes logic 1 (0). Three different threshold voltages for the circuit are V_1 = 1.9 V, V_2 = 2.5 V, and V_{13} = 3.0 V. In fact, the threshold voltage of the IC has hysteresis, meaning the threshold voltage is higher (lower) from 0-to-1 (1-to-0) output change. As the capacitance of the storage device is 330 µF for the proposed system, the change of the voltage due to difference in the energy level is within millivolt. An inverting

amplifier with the gain of 100 amplifies such small voltage gradient before voltage detection ICs.

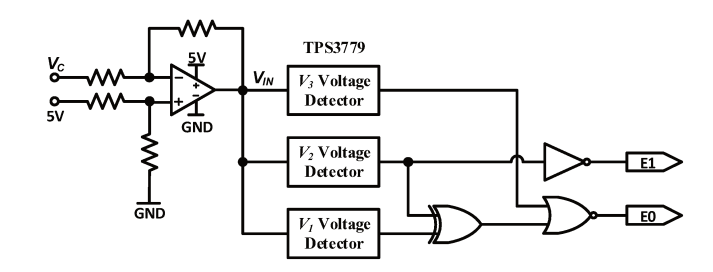


Fig. 6. Energy level indicator.

IV. EXPERIMENTAL RESULTS

This section describes experiment setup for the proposed system and reports energy for each energy source.

A. Experiment Setup

Fig. 7. Shows energy harvesting transducers for the proposed system, and Table I summaries the models and the operating conditions. The size of the PZT cantilever is 5.5 cm by 2.3 cm, the size of the TEG 4 cm by 4 cm, and the PV cell 4.5 cm by 4 cm.



Fig. 7. Energy transducers.

TABLE I. ENERGY HARVESTERS AND OPERATING CONDITIONS

Energy Type	Material	Operation Condition
Vibration	Mide	23 grams tip mass with 0.6 g acceleration
	PPA-1001	vibrating at 15 Hz
Thermal	TEG2- 126LDT	Temperature gradient at 5 °C
Solar	SOL3N	Solar simulator with 50,000 lux

Fig. 8. shows the experiment setup. A shaker is used to simulate the operating environment for the vibration energy. A heat plate and a fan are used to provide the temperature gradient of 5 °C for the TEG. fan, and a thermocouple are used to achieve 5 °C temperature gradient for the thermal energy. A solar simulator is used to emulate outdoor sunlight. Note that luminance of direct sunlight ranges from 32,000 to 100,000 Lux.

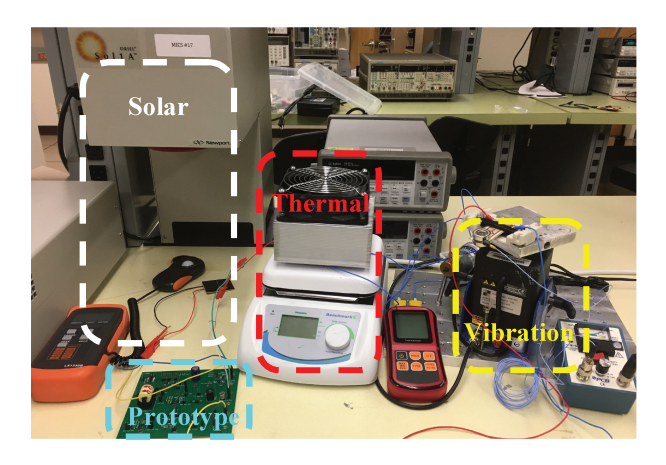


Fig. 8. Energy transducers.

B. Vibration Energy Harvesting

The PZT cantilever with 23 g of tip mass is set to vibrate under 0.6 g acceleration at 15 Hz resonant frequency. A variable resistor is connected to the NVC output to obtain the optimal resistance of the PZT cantilever, and we observed that the optimal resistance is 80 k Ω with peak power of 4.52 mW. To emulate the optimal resistance, the duty cycle for PZT buck-boost converter is obtained as 2.9 % using (1) for the inductance of 22 mH and the switching frequency of 1.52 kHz. The output power at the load resistance of the buck-boost converter it plotted in Fig. 9. The peak power of 2.61 mW is delivered to 3 k Ω , and the peak efficiency is 57.7 %. It is interesting to note that output power is sensitive to the load resistance, although the emulated input resistance of the buck-boost converter is independent from (1).

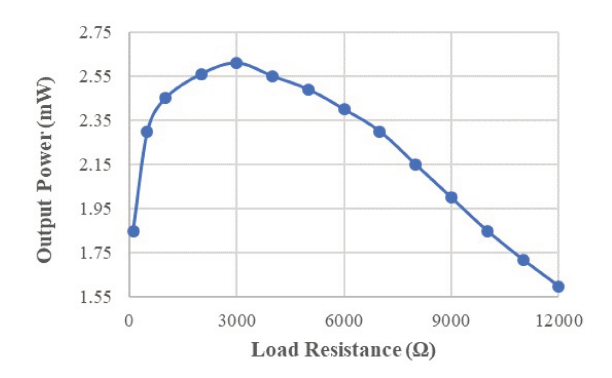


Fig. 9. Output power for PZT.

C. Thermal Energy Harvesting

A variable resistor is connected at the output of the TEG, and we observed that the optimal resistance is 5.5 Ω with peak power of 5.22 mW under 5 °C temperature gradient. To emulate the optimal resistance, the duty cycle for the TEG buck-boost converter is obtained as 45.2 % using (1) for the inductance of 390 μ H and the switching frequency of 1.44 kHz. The output power at the load resistance of the buck-boost converter it plotted in Fig. 10. The peak power of 2.9 mW is delivered to 3 k Ω , and the peak efficiency is 55.6 %. Like the

PZT cantilever, the power is rather sensitive to the load resistance.

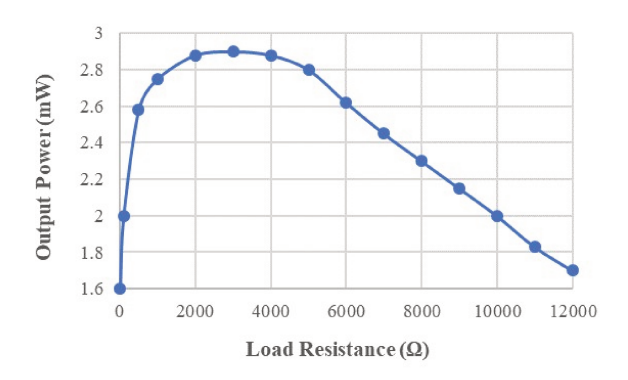


Fig. 10. Output power for TEG.

D. Solar Energy Harvesting

A variable resistor is connected at the output of the solar panel, and we observed that the optimal resistance is 1100 Ω with peak power of 54.12 mW under the illuminance of 50,000 Lux. The output power at the load resistance of the BQ25504 IC is plotted in Fig. 11. The peak power of 39.0 mW is delivered to 910 Ω , and the peak efficiency is 80 %. The power increases sharply as the resistance increase from 800 Ω to 900 Ω and then decreases rather slowly after the peak. This result is consistent to the maximum achievable efficiency provided by the datasheet [18].

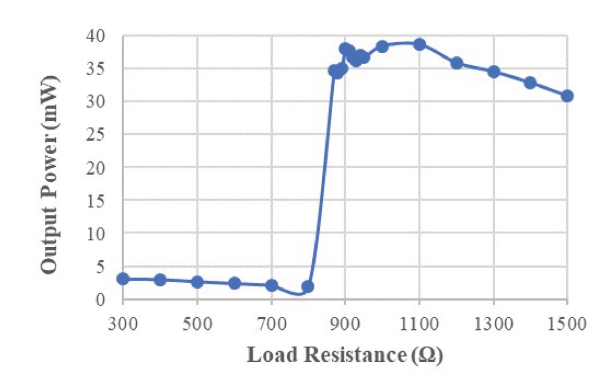
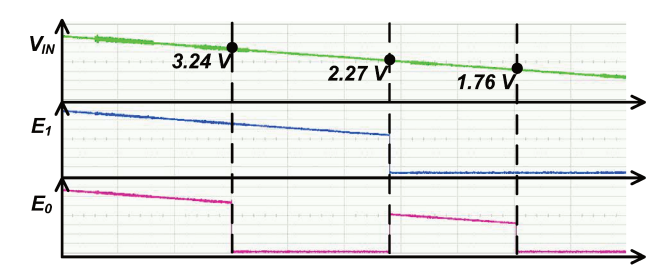


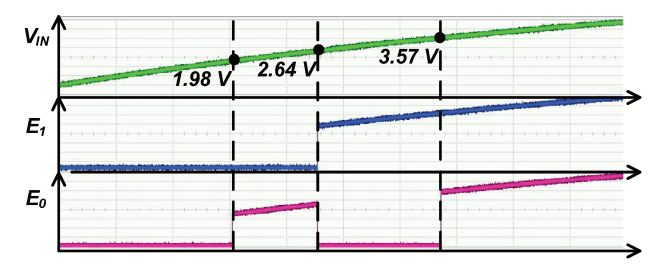
Fig. 11. Output power for PV cell.

E. Energy Level Indicator

The energy harvested from the three energy sources is stored in the same capacitor C_B . The energy level indicator senses the capacitor voltage and presents the voltage level in four different steps. The waveforms in Fig.12. show the inputs and outputs of the TPS3779 voltage detectors during the capacitor charging and discharging periods. Each voltage has an internal hysteresis of 10%, and the threshold voltage for switch on and switch off between adjacent states is labeled in Fig. 12. The power consumption of the energy level indicator is $60~\mu W$.



(a) Capacitor charging period



(b) Capacitor discharging period

Fig. 12. Digital output waveforms.

V. CONCLUSIONS

The proposed system harvests vibration, thermal, and solar energy from automobiles, which aims to power a microcontroller (MCU) for cryptography. The building blocks for vibration and thermal energy harvesting adopt resistive impedance matching and the IC for solar energy harvesting adopts maximum power point tracking. The PZT cantilever delivers peak power of 2.61 mW at the resonant frequency of 15 Hz with 0.6 g acceleration. The TEG delivers peak power of 2.9 mW for the thermal gradient of 5 °C, and the PV cell deliver 39.0 mW under the under the illuminance of 50,000 Lux. The experimental results indicate that the amount of solar energy is far higher than the other two sources. The energy level indicator shows the energy level of the storage device, which can be utilized by an MCU for cryptography to increase the data rate and/or decrease the latency.

ACKNOWLEDGMENT

This research was supported in part by the National Science Foundation Award no 1704176.

REFERENCES

- "Gartner Says 6.4 Billion Connected 'Things' Will Be in Use in 2016, Up 30 Percent From 2015." [Online]. Available: http://www.gartner.com/newsroom/id/3165317.
- [2] "More Than 30 Billion Devices Will Wirelessly Connect to the Internet of Everything in 2020." [Online]. Available: https://www.abiresearch.com/press/more-than-30-billion-devices-willwirelessly-conne/.

- [3] S. Bandyopadhyay and A. P. Chandrakasan, "Platform Architecture for Solar, Thermal, and Vibration Energy Combining With MPPT and Single Inductor," Journal of Solid-State Circuits, vol. 47, no. 9, pp. 2199-2215, Sept. 2012.
- [4] C. Ding, S. Heidari, Y. Wang, Y. Liu and J. Hu, "Multi-source in-door energy harvesting for non-volatile processors," International Symposium on Circuits and Systems (ISCAS), pp. 173-176, 2016.
- [5] M. Alhawari, T. Tekeste, B. Mohammad, H. Saleh and M. Ismail, "Power management unit for multi-source energy harvesting in wearable electronics," 2016 IEEE 59th International Midwest Symposium on Circuits and Systems (MWSCAS), Abu Dhabi, 2016, pp. 1-4.
- [6] J. H. Hyun, L. Huang and D. S. Ha, "Vibration and Thermal Energy Harvesting System for Automobiles with Impedance Matching and Wake-up," International Symposium on Circuits and Systems (ISCAS), pp. 1-5, 2018.
- [7] S. Huang and D. Infield, "The potential of domestic electric vehicles to contribute to Power System Operation through vehicle to grid technology," 2009 44th International Universities Power Engineering Conference (UPEC), Glasgow, 2009, pp. 1-5.
- [8] N. S. Shenck and J. A. Paradiso, "Energy scavenging with shoe-mounted piezoelectrics," in IEEE Micro, vol. 21, no. 3, pp. 30-42, May-June 2001.
- [9] N. Chen, T. Wei, D.S. Ha, H.J. Jung, and S. Lee, "Alternating Resistive Impedance Matching for an Impact-Type Micro Wind Piezoelectric Energy Harvester," IEEE Transactions on Industrial Electronics, Vol. 65, No. 9, pp. 7374 - 7362, September 2018.
- [10] J.H. Hyun, N. Chen, and D.S. Ha, "Energy Harvesting Circuit for Road Speed Bumps Using a Piezoelectric Cantilever," 44th Annual Conference of the IEEE Industrial Electronics Society (IECON 2018), October 2018.
- [11] J. Wang, A. Dancy, and D.S. Ha, "Vibration Energy Harvesting Circuit with Impedance Matching and Wake-up for Freight Railcars," 44th Annual Conference of the IEEE Industrial Electronics Society (IECON 2018), October 2018.
- [12] Charles Suslowicz, Archanaa S Krishnan, Patrick Schaumont, "Optimizing Cryptography in Energy Harvesting Applications," Workshop on Attacks and Solutions in Hardware Security (ASHES), pp. 17-26. October 2017.
- [13] Ying-Tung Hsiao and China-Hong Chen, "Maximum power tracking for photovoltaic power system," Conference Record of the 2002 IEEE Industry Applications Conference. 37th IAS Annual Meeting (Cat. No.02CH37344), Pittsburgh, PA, USA, 2002, pp. 1035-1040 vol.2.
- [14] S. Priya, H.-C. Song, Y. Zhou, R. Varghese, A. Chopra, S.-G. Kim, I. Kanno, L. Wu, D.S Ha, J. Ryu, R.G. Polcawich, "A Review on Piezoelectric Energy Harvesting: Materials, Methods, and Circuits," Energy Harvesting and Systems, Vol. 4, No. 1, pp. 3 39, March 2017.
- [15] I. M. Darmayuda et al., "A Self-Powered Power Conditioning IC for Piezoelectric Energy Harvesting From Short-Duration Vibrations," in IEEE Transactions on Circuits and Systems II: Express Briefs, vol. 59, no. 9, pp. 578-582, Sept. 2012.
- [16] N. Kong and D. S. Ha, "Low-Power Design of a Self-powered Piezoelectric Energy Harvesting System With Maximum Power Point Tracking," in IEEE Transactions on Power Electronics, vol. 27, no. 5, pp. 2298-2308, May 2012.
- [17] N. Kong, D. S. Ha, A. Erturk, and D. J. Inman, "Resistive impedance matching circuit for piezoelectric energy harvesting," Journal of Intelligent Material Systems and Structures, vol. 21, no. 13, pp. 1293– 1302, 2010.
- [18] "bq25504 Ultra Low-Power Boost Converter With Battery Management for Energy Harvester Applications," Ti.com, 2018. [Online]. Available: http://www.ti.com/lit/ds/symlink/bq25504.pdf